Phys Chem Minerals (2003) 30: 511–516
DOI 10.1007/s00269-003-0353-z

ORIGINAL PAPER

H. Fukui · O. Ohtaka · T. Suzuki · K. Funakoshi

Thermal expansion of $Mg(OH)_2$ brucite under high pressure and pressure dependence of entropy

Received: 20 January 2003/ Accepted: 14 July 2003

Abstract An equation of state for $Mg(OH)_2$ brucite under high-pressure and high-temperature conditions has been obtained by measuring temperature dependence of volume up to 600 K at ambient pressure and pressure dependence of volume up to 16 GPa at 300, 473, 673, and 873 K with in situ X-ray diffraction. Pressure dependence of entropy of brucite has been calculated with thermal expansion coefficient and volume which are derived from the present EoS. This dependence indicates that generation of secondary OH dipoles affects entropy. The OH dipoles probably appear around 2 GPa and the number seems not to change over 8 GPa at 300 K.

Keywords Brucite · Equation of state · Thermal expansion · Entropy · X-ray diffraction

Introduction

$Mg(OH)_2$ brucite is one of the simplest solids which have hydroxyl groups. It has a hexagonal crystal structure (Zigan and Rothbauer 1967) with space group $P\bar{3}m1$. Brucite has been studied to understand hydrogen behavior and the nature of hydrogen bonding in solid and to understand the compression behavior of layered dense magnesium hydrous silicates (DMHS) because an $Mg(OH)_6$ unit is regarded as a part of a DMHS structure (Kudoh et al. 1993).

Spectroscopy techniques (Kruger et al. 1989; Duffy et al. 1995; Shinoda and Aikawa 1998; Shinoda et al. 2002) and neutron diffraction (Parise et al. 1994) were applied to $Mg(OH)_2$ and $Mg(OD)_2$ in order to investigate the behavior of hydrogen and deuteron, respectively. Both types of experiments showed that a secondary OH dipole is formed with compression and that hydrogen prefers the 6*i* position to the 2*d*, which hydrogen occupies under ambient conditions. The site change of hydrogen from 2*d* to 6*i* was also reported on $Ca(OH)_2$ (Desgranges et al. 1993). The effect of the change of hydrogen site in $Ca(OH)_2$ appeared on the thermal expansion coefficient at one-atmosphere condition. The site change is called hydrogen motion.

Equations of state (EoS) for brucite were reported using X-ray diffraction by many groups (Fei and Mao 1993; Catti et al. 1995; Duffy et al. 1995; Xia et al. 1998; Nagai et al. 2000). There is, however, no report that a hydrogen behavior such as mentioned above affects the lattice system of brucite. One of the reasons is that only its compression behavior was discussed so far. The effect may appear as a thermal effect on the lattice system just as reported for portlandite (Fukui et al. 2003). The thermal expansion has to be determined precisely in order to discuss the effect.

We report the thermo-elastic properties of $Mg(OH)_2$ brucite obtained through in situ X-ray observations at high temperature and high pressure. Using these results, the temperature dependence of thermal expansion at constant pressure is discussed.

H. Fukui (✉) · O. Ohtaka
Department of Earth and Space Science,
Osaka University, Toyonaka, Osaka 560–0043, Japan
e-mail: fukuih@ess.sci.osaka-u.ac.jp
Tel.: +81–6-6850–5803
Fax: +81–6-6850–5480

T. Suzuki
Faculty of Environmental Engineering,
The University of Kitakyushu, Hibikino,
Fukuoka 808–0135, Japan

K. Funakoshi
Japan Synchrotron Radiation Research Institute,
SPring-8, Hyogo 678–5198, Japan

Experimental

Ambient pressure experiments

To obtain reference volumes at ambient pressure, V_0, which is a parameter for EoS, X-ray diffraction observations at high temperature were carried out with XRD-DSC II (Rigaku Corp). The degree of temperature fluctuation is below 0.2 K. Temperature

calibrations were performed by detecting the melting reactions of indium (429.81 K), tin (505.168 K), and lead (600.702 K). The optical system was refined using a silicon diffraction pattern with Cu $K\alpha_1$ radiation.

The dehydration temperature was confirmed before X-ray observations. X-ray diffraction patterns were collected from just below the dehydration temperature to room temperature at about every 50 K. Commercial reagent of 99.9% purity $Mg(OH)_2$ powder with brucite structure produced by Iwatani Chemical Ltd. was used as a starting sample. X-ray diffraction patterns were collected at air–atmosphere condition. The sample was filled into an aluminum plate. The heating/cooling rate for this experiment was 5 $Kmin^{-1}$.

High-pressure experiments

In situ X-ray diffraction observations under high pressure were done up to 23 GPa at 300 K and to 16 GPa at higher temperature using the SPEED-1500 system installed at BL04B1, SPring-8 (Utsumi et al. 1998). Eight tungsten carbide cubes with truncation edge length of 3 mm were used as the second-stage anvils. The pressure-transmitting medium was sintered magnesium oxide and the gasket material was pyrophillite. A cell assemblage of Irifune et al. (1998) was used with modifications. In order to prevent the sample from reacting with the pressure medium of magnesium oxide, we introduced a sample chamber made of graphite which was confirmed in advance not to react with brucite up to 6 GPa and 1500 K. Figure 1 shows the central part of the cell. The sample chamber was put between a pair of heater sheets made of cemented TiC-diamond powders. The starting material was a mixture of brucite and gold powders [$Mg(OH)_2$: Au = 10:1 in weight ratio]. Initial diameters of the capsule were 2 mm inside and 3 mm outside. Disks of magnesium oxide were put between the graphite capsule and TiC heaters for electric insulation. White X-rays collimated by horizontal (0.05-mm) and vertical (0.1-mm) slits were directed to a sample position very close to the junction of a thermocouple. The position was confirmed with X-ray radiography using a CCD camera. The diffracted beam, collimated by a 0.05-mm horizontal slit, was detected with a pure germanium solid-state detector attached on a horizontal rotating goniometer. The data collection was performed with typical duration of 600 s at the two-theta angle of 4.7°. Pressure was estimated from the unit-cell volume of gold using the equation of state (Anderson et al. 1989). Temperature was monitored with a thermocouple of W97%Re3%–W75%Re25%. Pressure effects on emf were ignored. Temperature fluctuation was less than 1 K during the exposure time. The sample was compressed and then heated to 900 K and kept at that temperature for more than 10 min. Diffraction patterns were collected on a cooling cycle. Because deviatoric stress relaxed once the sample was heated above the target temperature, the obtained data were free from such complicating effects.

Results and discussion

Thermal expansion at ambient pressure

The dehydration temperature of brucite was determined to be 600.6 K. A representative X-ray diffraction pattern is shown in Fig. 2. Lattice constants were refined with four diffraction lines from (001), (100), (101), and (102) planes using the least-squares method. Calculated lattice parameters, the unit-cell volume, and c/a ratio are shown in Table 1 and plotted in Fig. 3. The values of a and c vary smoothly in this temperature range. The c/a ratio also varies continuously. The datasets from 299 to 592 K were used to calculate the thermal expansion coefficients. The coefficients were calculated with the following equation:

$$l = l_0 \exp\left[\int_{T_0=300K}^{T} \alpha_l \, dT\right], \quad (1)$$

where l is a length of a, or c, or volume, and l_0 is its value at the standard temperature, T_0. T_0 is 300 K in this study. α is a thermal expansion coefficient. Obtained values of a, c, and volume are listed in Table 2. The obtained thermal expansion coefficient for volume is shown with previous results in Table 3. Though the values are very similar around 300 K, that by Redfern and Wood (1992) is considerably larger at the high-temperature region than those of the others. They reported that the lattice parameters at 293 K were 3.149 and 4.749 Å for the a axis and c axis, respectively. The value of the a axis is larger than reported by the others and those of JCPDS, while that of the c axis is smaller. This fact means that Redfern and Wood underestimated the unit-cell volume at the standard state. Consequently, the thermal expansion coefficient was overestimated.

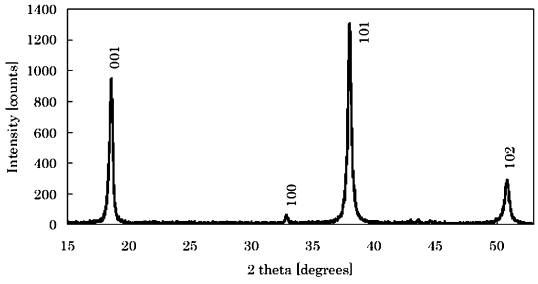

Fig. 2 X-ray profile of $Mg(OH)_2$ obtained at 299.5 K and ambient pressure

Table 1 Refined lattice parameters and volume of brucite under ambient conditions

T (K)[a]	a (Å)	c (Å)	c/a	V (Å^3)
299.3	3.1476(4)[a]	4.7705(6)	1.5156	40.930(12)
299.3	3.1477(7)	4.7694(10)	1.5152	40.925(22)
349.2	3.1481(16)	4.7807(25)	1.5186	41.031(47)
356.4	3.1486(13)	4.7867(15)	1.5203	41.096(37)
397	3.1490(7)	4.7902(10)	1.5212	41.136(22)
418	3.1507(3)	4.7979(4)	1.5228	41.247(10)
456.6	3.1514(11)	4.8098(13)	1.5262	41.367(31)
469.8	3.1521(6)	4.8063(8)	1.5248	41.356(18)
515.1	3.1532(2)	4.8215(2)	1.5291	41.516(5)
571.5	3.1549(7)	4.8348(9)	1.5325	41.675(20)
592.9	3.1550(8)	4.8411(10)	1.5344	41.732(23)

[a] *Figures in parentheses* indicate estimated standard deviations of the last significant digit

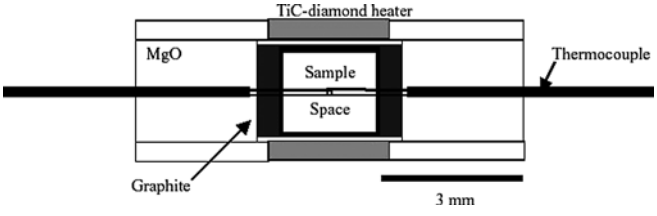

Fig. 1 Central part of the high pressure cell. Heaters are placed below and above the sample space. Other parts are shown in the figure

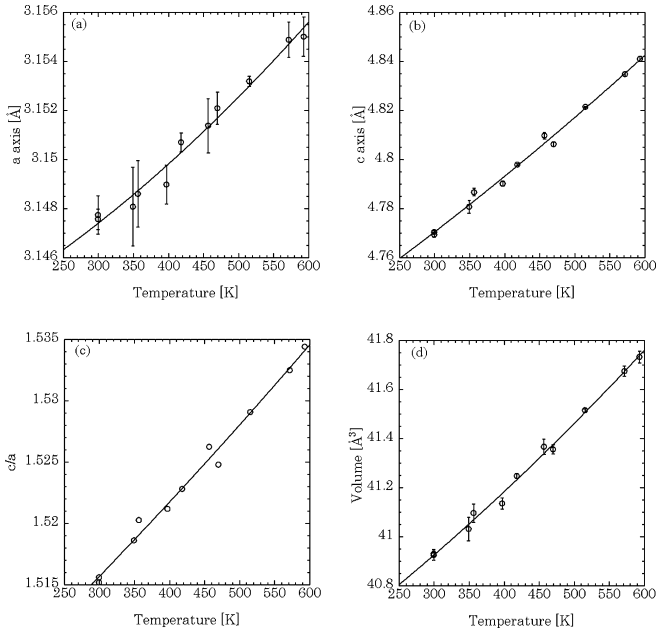

Fig. 3a–d Axial and volume data of $Mg(OH)_2$ as function of temperature at ambient pressure. **a** *a* axis. **b** *c* axis. **c** *c*/*a* ratio. **d** Volume

Those by the others are consistent even at high temperature.

Isothermal elastic properties

A representative diffraction pattern of $Mg(OH)_2$ brucite acquired at high pressure is shown in Fig. 4. Lattice parameters of $Mg(OH)_2$ under each condition were derived from *d* values for at least four lines out of (001), (100), (101), (102), (110), and (111) planes. Obtained lattice parameters at 300 K are listed in Table 4. The volume compression data are plotted in Fig. 5. The bulk modulus and its pressure derivative at zero pressure can be calculated by fitting the third-order Birch–Murnaghan equation of state (Birch 1947) to the pressure–volume data:

$$P = \frac{3}{2}K_0\left[\left(\frac{V_0}{V}\right)^{\frac{7}{3}} - \left(\frac{V_0}{V}\right)^{\frac{5}{3}}\right] \cdot \left\{1 + \frac{3}{4}(K_0' - 4)\cdot\left[\left(\frac{V_0}{V}\right)^{\frac{2}{3}} - 1\right]\right\}. \quad (2)$$

The calculated bulk modulus and its pressure derivative are shown in Table 5 with previous results. The calculated compression curve and previous data are also shown in Fig. 5. The results of room temperature compression are consistent with each other.

Data obtained under high-temperature and high pressure conditions are listed in Table 4 and plotted in Fig. 6. Equation (2) was fitted to the compression data with fixed V_0 values which are calculated with thermal expansion at ambient pressure. Obtained isothermal elastic parameters, K_{T0} and K_{T0}' are listed in Table 6. The compression curves are also shown in Fig. 6. These curves show good agreement with measured volumes. Figure 6 also shows pressure–volume data reported by Xia et al. (1998) with open squares and their compression curves with dotted lines. Both curves of the present result and their result are very consistent, whereas there is a difference between the curves at 873 K at the low-pressure region as shown in Fig. 6c. We believe that the present observation is more accurate than that by Xia et al. (1998) for the following reasons. (1) Pressure marker was mixed with sample. (2) The thermocouple junction was located at the center of the sample. (3) The temperature fluctuation and gradient are very small. (4) Obtained diffraction data came from an area very close to the junction.

Temperature dependence of bulk modulus and its pressure derivative at ambient pressure were calculated by fitting the following equation $B = (\partial B/\partial T)_{P=0} \cdot (T-300) + B_{T=300}$, where B, $(\partial B/\partial T)_{P=0}$, and $B_{T=300}$ show K_{T0} or K_{T0}', the temperature derivative at zero pressure, and the value at 300 K, respectively. Consequently, the value of $(\partial K_T/\partial T)_{P=0}$ was obtained as −0.0319(29) and that of $(\partial K_T'/\partial T)_{P=0}$ as 0.00571(45).

Table 2 Obtained lattice constants and volume of brucite at 300 K

a_0 [Å]	3.1472(2)
c_0 [Å]	4.7699(11)
V_0 [Å^3]	40.917(12)

Pressure dependences of thermal expansion coefficient and entropy

Thermal expansion coefficients at constant pressure were obtained by fitting Eq. (1) to four volumes under each

Table 3 Thermal expansion coefficients of brucite[a]

α_0 ($\times 10^{-5}$ 1 K^{-1})	α_1 ($\times 10^{-7}$ 1 K^{-2})	Temperature range (K)	Reference
0.23	2.37	293–583	Redfern and Wood (1992)
8.0	–	300–650	Fei and Mao (1993)
7.3	0.36	–	Xia et al. (1998)
6.69(18)[b]	–	299–592	This study

[a] Thermal expansion coefficient is expressed as $\alpha = \alpha_0 + \alpha_1 T$. Redfern and Wood (1992) originally reported it as $\alpha = \alpha_0 + \alpha_1(T - 273)$
[b] Figure in parentheses indicates estimated standard deviations of the last significant digit

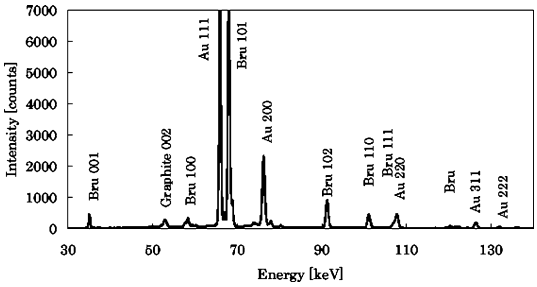

Fig. 4 X-ray diffraction profile of $Mg(OH)_2$ obtained at 300 K and 16.05 GPa. *Bru* and *Au* indicate diffraction lines from $Mg(OH)_2$ brucite and gold, respectively

pressure condition. These volumes were calculated with the elastic parameters shown in Table 5.

Since the thermal expansion coefficient has been obtained, we can calculate the pressure dependence of entropy at constant temperature using a relation $(\partial S/\partial P)_T = -\alpha V$, where S, P, T, ∂, and V are entropy, pressure, temperature, thermal expansion coefficient, and volume, respectively. The obtained values are plotted in Fig. 7. $(\partial S/\partial P)_T$ has large negative values under lower pressure conditions. As pressure increases, the absolute value decreases. The slope of $(\partial S/\partial P)_T$ at 300 K is almost constant from ambient pressure to 2 GPa and becomes smaller from 3 to 7 GPa. Above 8 GPa, $(\partial^2 S/\partial P^2)_T$ is a little negative or almost zero. The pressure range where the gradient changes is consistent with the pressure where a newly IR absorption peak appears (Shinoda and Aikawa 1998). These results imply the following:

1. Entropy decreases with pressure.
2. The absolute value of $(\partial S/\partial P)_T$ is large below 3 GPa and decreases above this pressure. This can be understood by considering two pressure effects on configuration and vibration of the OH dipole. Contribution of configurational entropy increases with pressure because the hydrogen atoms that form the secondary OH dipole occupy one of three 6*i* sites. Because the frequency of the secondary OH bonding is smaller than that of the original OH bonding and the vibrational entropy change is expressed as $\Delta S = k_B \ln(v/v') \cdot \text{oscillator}^{-1}$, where k_B is the Boltzman constant, when the frequency changes from v to v', the frequency decrease from original OH to secondary OH causes entropy to increase. Both effects of configuration and vibration involved with the

Table 4 Refined lattice parameters and volume of brucite

T (K)	P (GP_a)	a (Å)	c (Å)	c/a	V (Å^3)
300	−0.06(13)[a]	3.1450(12)	4.7773(31)	1.5190	40.922(43)
300	0.00(6)	3.1445(15)	4.7773(26)	1.5192	40.909(50)
300	4.00(7)	3.0990(10)	4.5773(24)	1.4771	38.069(32)
300	5.80(6)	3.0791(5)	4.5002(11)	1.4615	36.950(15)
300	7.32(8)	3.0643(5)	4.4588(12)	1.4551	36.258(16)
300	7.50(13)	3.0702(71)	4.4424(160)	1.4470	36.264(212)
300	10.35(10)	3.0380(8)	4.3984(17)	1.4478	35.156(24)
300	13.44(13)	3.0141(2)	4.3421(6)	1.4406	34.162(7)
300	14.38(11)	3.0101(14)	4.3384(31)	1.4413	34.043(40)
300	16.05(12)	2.9971(9)	4.3166(21)	1.4403	33.579(27)
300	18.26(15)	2.9824(23)	4.2836(58)	1.4363	32.996(64)
300	19.86(10)	2.9662(19)	4.2657(43)	1.4381	32.502(53)
300	22.56(12)	2.9532(14)	4.2444(33)	1.4372	32.058(41)
473	9.59(11)	3.0448(19)	4.4055(37)	1.4469	35.371(54)
473	11.36(9)	3.0294(10)	4.3651(33)	1.4409	34.694(34)
473	13.43(12)	3.0148(32)	4.3464(74)	1.4417	34.212(93)
473	15.15(15)	3.0027(26)	4.3064(49)	1.4342	33.626(70)
473	16.52(7)	2.9907(80)	4.2957(211)	1.4364	33.437(242)
473	5.95(3)	3.0780(3)	4.4953(7)	1.4605	36.883(10)
473	8.28(7)	3.0584(168)	4.4548(319)	1.4566	36.088(474)
473	10.24(5)	3.0411(29)	4.3967(56)	1.4458	35.214(81)
673	9.07(6)	3.0520(28)	4.4291(66)	1.4512	35.729(85)
673	11.00(5)	3.0350(29)	4.3861(40)	1.4451	34.979(75)
673	13.05(5)	3.0222(2)	4.3510(5)	1.4397	34.416(7)
673	14.56(6)	3.0043(42)	4.3274(56)	1.4404	33.826(104)
673	16.09(12)	2.9985(33)	4.3211(116)	1.4411	33.647(117)
673	5.62(5)	3.0852(11)	4.5225(32)	1.4659	37.280(38)
673	7.96(5)	3.0629(9)	4.4600(39)	1.4561	36.235(38)
673	9.85(6)	3.0441(29)	4.4144(47)	1.4502	35.426(77)
873	8.75(4)	3.0540(8)	4.4670(19)	1.4627	36.081(24)
873	10.46(3)	3.0367(7)	4.4172(21)	1.4546	35.276(24)
873	12.44(11)	3.0237(16)	4.3887(22)	1.4515	34.749(31)
873	14.00(9)	3.0080(36)	4.3748(126)	1.4544	34.280(128)
873	15.48(5)	3.0010(37)	4.3451(51)	1.4479	33.890(72)
873	5.21(5)	3.0875(7)	4.5660(19)	1.4789	37.695(23)
873	7.52(4)	3.0659(8)	4.4951(23)	1.4662	36.593(26)
873	9.49(6)	3.0493(14)	4.4519(27)	1.4600	35.848(39)

[a] Figures in parentheses for lattice parameters and volume indicate estimated standard deviations of the last significant digit. Those for pressure were errors estimated from the standard deviations of the lattice parameter of gold

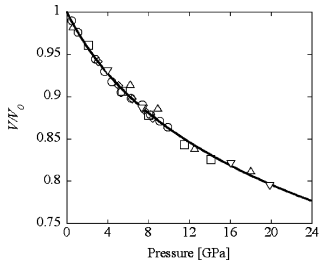

Fig. 5 Volume compression data shown by *inverted triangles* and compression curve of brucite at 300 K in this study. Previous results are shown by *circles* (Catti et al. 1995); *squares* (Duffy et al. 1995); *diamonds* (Xia et al. 1998), and *triangles* (Nagai et al., 2000)

Table 5 Bulk moduli and their pressure derivatives of brucite at 300 K

K_{T0} (GPa)	K_{T0}'	Method	Reference
54.3	4.7	PXD[a]	Fei and Mao (1993)
47	4.7 (fixed)	PND[b]	Parise et al. (1994)
42	5.7	SCXD[c]	Duffy et al. (1995)
39	7.6	PND	Catti et al. (1995)
36.7	–	B[d]	Xia et al. (1998)
39.6	6.7	PXD	Xia et al. (1998)
44	6.7 (fixed)	PXD	Nagai et al. (2000)
41.8(1.3)	6.6(3)	PXD	This study

[a] PXD Powder X-ray diffraction
[b] PND Powder neutron diffraction
[c] SCXD Single-crystal X-ray diffraction
[d] B Brillouin scattering

hydrogen transition therefore make the absolute value of $(\partial S/\partial P)_T$ decrease.

3. The value does not change much above 8 GPa. This means that all hydrogen atoms have formed the secondary OH dipole.

The variation $(\partial S/\partial P)_T$ for brucite has been compared with that for periclase, into which brucite dehydrates, and which does not have a phase transition in this pressure range. The values for periclase were calculated with the reported parameters (Dewaele et al. 2000). These are shown also in Fig. 7. There is no slope change on $(\partial S/\partial P)_T$ though the value decreases little by little with pressure due to the effect of pressure on the vibration. This is consistent with the fact that no phase transition has so far been reported for periclase in this pressure range.

Through these experiments, hydrogen behavior obviously has been found to affect the lattice system. This transition of hydrogen in brucite is not a first-order phase transition but a higher one. It is, however, not mentioned what the order the transition is. Though $(\partial^2 S/\partial P^2)_T$ seems not to show discontinuity at any pressure but to change continuously because smooth functions were used to model the relationship between volume, pressure, and temperature, there is still a possibility that $(\partial^2 S/\partial P^2)_T$ has a discontinuity. To confirm this more precise measurement, that is probably very difficult with the present instruments, is needed.

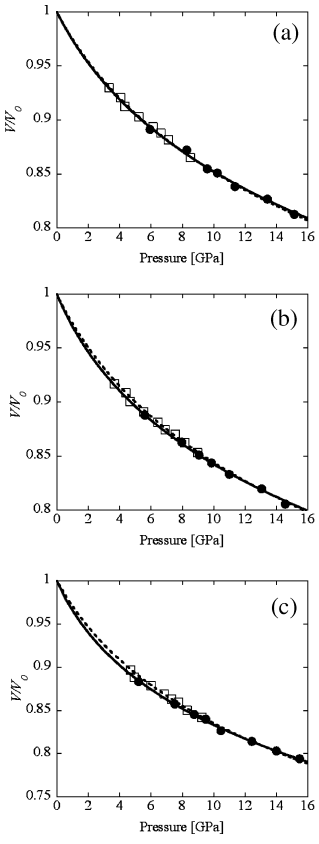

Fig. 6a–c Volume compression data of brucite under high-temperature conditions **a** 473 K. **b** 673 K. **c** 873 K. *Solid circles* and *curves* indicate the results of this study, and *open squares* and *dotted curves* are those from Xia et al. (1998)

Table 6 Isothermal bulk moduli and the pressure derivatives of brucite at high temperature

T (K)	K_{T0} (GPa)	K'_{T0}
300	41.8(1.3)	6.6(4)
473	32.6(2.5)	8.3(1.1)
673	28.8(2.1)	9.0(1.1)
873	23.9(1.4)	10.0(0.9)

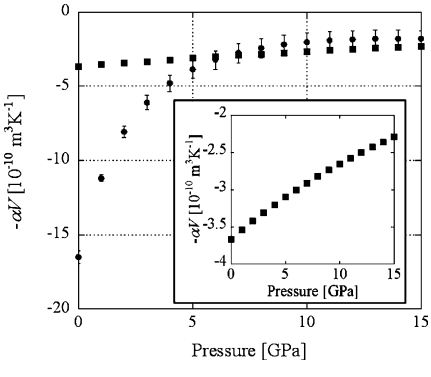

Fig. 7 Pressure derivative of entropy at 300 K. *Circles* and *squares* are for brucite and for periclase, respectively. The *inset* shows the values for periclase

Conclusion

The EoS for brucite has been determined precisely in the range up to 16 GPa and 900 K and thermal expansion coefficients under high-pressure conditions were obtained from the EoS. Obtained values of $-\alpha V$, which is the same as pressure dependence of entropy, show that the hydrogen motion certainly affects the lattice system. It is likely that the number of the secondary OH bonding increases from around 2 GPa and does not change beyond 8 GPa at 300 K.

Acknowledgements The authors thank to Dr. A. Pavese and an anonymous referee for their valuable comments and careful reading. The authors appreciate the help of Mr. H. Takebe and Mr. H. Arima in situ X-ray measurements under pressure. The X-ray diffraction studies at BL04B1 in SPring-8 were performed with the approval of the Japan Synchrotron Radiation Research Institute (JASRI) (proposal no. 2001B0057-ND-np). This research is partially supported by JSPS research fellowships for young scientists.

References

Anderson OL, Isaak DG, Yamamoto S (1989) Anharmonicity and the equation of state for gold. J Appl Phys 65: 1534–1543

Birch F (1947) Finite elastic strain of cubic crystals. Phys Rev 71: 809–824

Catti M, Ferraris G, Hull S, Pavese A (1995) Static compression and H disorder in brucite, $Mg(OH)_2$, to 11 GPa: a powder neutron diffraction study. Phys Chem Miner, 22: 200–206

Desgranges L, Grebille D, Calvarin G (1993) Hydrogen thermal motion in calcium hydroxide: $Ca(OH)_2$. Acta Crystallogr(B) 49: 812–817

Dewaele A, Fiquet G, Andrault D, Hausrmann D (2000) *P–V–T* equation of periclase from synchrotron radiation measurements. J Geophys Res 105: 2869–2877

Duffy TS, Shu J, Mao HK, Hemley RJ (1995) Single-crystal X-ray diffraction of brucite to 14 GPa. Phys Chem Miner 22: 277–281

Fei Y, Mao HK (1993) Static compression of $Mg(OH)_2$ to 78 GPa at high temperature and constraints on the equation of state of fluid H_2O. J Geophys Res 98: 11875–11884

Fukui H, Ohataka O, Fujisawa T, Kunisada T, Suzuki T, Kikegawa T (2003) Thermo-elastic property of $Ca(OH)_2$ portlandite. High-Pressure Res 23: 55–61

Irifune T, Nishiyama N, Kuroda K, Inoue T, Isshiki M, Utsumi W, Funakoshi K, Urakawa S, Uchida T, Katsura T, Ohtaka O (1998) The postspinel phase boundary in Mg_2SiO_4 determined by *in-situ* X-ray diffraction. Science 279: 1698–1700

Kruger MB, Williams Q, Jeanloz R (1989) Vibrational spectra of $Mg(OH)_2$ and $Ca(OH)_2$ under pressure. J Chem Phys 91: 5910–5915

Kudo h Y, Finger LW, Hazen RM, Prewitt CT, Kanzaki M, Veblen DR (1993) Phase-E a high-pressure hydrous silicate with unique crystal chemistry. Phys Chem Miner 19: 357–360

Nagai T, Hattori T, Yamanaka T (2000) Compression mechanism of brucite: an investigation by structural refinement under pressure. Am Mineral 85: 760–764

Parise JB, Leinnenweber K, Weidner DJ, Tan K, Von Dreele RB (1994) Pressure-induced H bonding: Neutron diffraction study of brucite, $Mg(OD)_2$, to 9.3 GPa. Am Mineral 79: 193–196

Redfern SAT, Wood BJ (1992) Thermal expansion of brucite, $Mg(OH)_2$. Am Mineral 77: 1129–1132

Shinoda K, Aikawa N (1998) Interlayer proton transfer in brucite under pressure by polarized IR spectroscopy to 5.3 GPa. Phys Chem Miner 25: 197–202

Shinoda K, Yamakata M, Nanba T, Kimura H., Moriwaki T, Kondo Y, Kawamoto T, Niimi N, Miyoshi N, Aikawa N (2002) High-pressure phase transition and behavior of protons in brucite $Mg(OH)_2$: a high-pressure-temperature study using IR synchrotron radiation. Phys Chem Miner 29: 396–402

Utsumi W, Funakoshi K, Urakawa S, Yamakata M, Tsuji K, Konishi H, Shimomura O (1998) SPring-8 beamlines for high-pressure science with multi-anvil apparatus. Rev High Pressure Sci Technol 7: 1484–1486

Xia X, Weidner DJ, Zhao H (1998) Equation of state of brucite: single-crystal brillouin spectroscopy study and polycrystalline pressure-volume-temperature measurement. Am Mineral 83: 68–74

Zigan F, Rothbauer R (1967), Neutronenbeugungsmessungen am Brucit. N J Mineral 137–143